A surface electromyography controlled steering assistance interface

Edric John Cruz Nacpil, Rencheng Zheng, Tsutomu Kaizuka and Kimihiko Nakano
Institute of Industrial Science, The University of Tokyo, Tokyo, Japan

Abstract

Purpose – Two-handed automobile steering at low vehicle speeds may lead to reduced steering ability at large steering wheel angles and shoulder injury at high steering wheel rates (SWRs). As a first step toward solving these problems, this study aims, firstly, to design a surface electromyography (sEMG) controlled steering assistance interface that enables hands-free steering wheel rotation and, secondly, to validate the effect of this rotation on path-following accuracy.

Design/methodology/approach – A total of 24 drivers used biceps brachii sEMG signals to control the steering assistance interface at a maximized SWR in three driving simulator scenarios: U-turn, 90° turn and 45° turn. For comparison, the scenarios were repeated with a slower SWR and a game steering wheel in place of the steering assistance interface. The path-following accuracy of the steering assistance interface would be validated if it was at least comparable to that of the game steering wheel.

Findings – Overall, the steering assistance interface with a maximized SWR was comparable to a game steering wheel. For the U-turn, 90° turn and 45° turn, the sEMG-based human–machine interface (HMI) had median lateral errors of 0.55, 0.3 and 0.2 m, respectively, whereas the game steering wheel, respectively, had median lateral errors of 0.7, 0.4 and 0.3 m. The higher accuracy of the sEMG-based HMI was statistically significant in the case of the U-turn.

Originality/value – Although production automobiles do not use sEMG-based HMIs, and few studies have proposed sEMG controlled steering, the results of the current study warrant further development of a sEMG-based HMI for an actual automobile.

Keywords Advanced driver assistance systems, Human–machine interface, Myoelectric control system, Path-following, Steering assistance system, Surface electromyography

Paper type Research paper

1. Introduction

Sometimes drivers have to steer sharply and rapidly at low vehicle speeds to maneuver in confined spaces such as narrow roads and crowded parking lots (Takada *et al.*, 2013). However, rapid, two-handed steering subjects the shoulder of the driver to high forces that may cause injury. If the steering wheel is rotated to the right with two hands from 0° to 65°, with an average time of 0.268 SD 0.065 s, healthy supraspinatus and deltoid muscles are subjected to forces that could lead to muscle overload (Pandis *et al.*, 2015).

The risk of injury is compounded by another issue at low speeds, namely, a decrease in the ability of the driver to turn a steering wheel, i.e. decreased steering portability. Primarily because of the reaction forces between the tires and the road, the torque required to steer the road wheels is maximized when an automobile is moving slowly or at a full stop (Ma *et al.*, 2016; Sharp and Granger, 2003). Consequently, when the steering wheel is manually rotated from the neutral position to 300° or higher, the ability of the driver to rotate the steering wheel decreases rapidly (Ma *et al.*, 2016).

As a means of preventing decreased steering portability and reducing the risk of shoulder injury, a steering assistance interface that relies on surface electromyography (sEMG) input from the biceps brachii muscles has been developed to produce rapid, hands-free steering wheel rotation for low speed, nonemergency driving tasks. Because the interface was designed to rotate steering wheels faster than healthy drivers, the major driving task of curve negotiation could have been significantly affected (Pauwelussen, 2015). The path-following accuracy of the interface during curve negotiation was thus validated by driving simulator trials at different steering wheel rates (SWRs). The fastest SWR setting was associated with acceptable path-following accuracy that was comparable overall to a game steering wheel.

The applications of previous steering assistance systems and how they differ from the current application are detailed in the next section. Section 3 offers an overview of the design of the steering assistance system and the adaptation of the system

The current issue and full text archive of this journal is available on Emerald Insight at: **www.emeraldinsight.com/2399-9802.htm**

Journal of Intelligent and Connected Vehicles
2/1 (2019) 1–13
Emerald Publishing Limited [ISSN 2399-9802]
[DOI 10.1108/JICV-11-2018-0011]

Received 6 November 2018
Revised 15 January 2019
Accepted 4 March 2019

interface to a driving simulator. Section 4 describes how drivers performed turning maneuvers with the interface so that the resulting trajectories could be used to determine path-following accuracy. A comparison in Section 5 is conducted between the interface and the game steering wheel with respect to path-following accuracy. Although the results of this comparison validate the accuracy of the steering assistance interface, there are limitations in this study that are conveyed in Section 6. Nevertheless, the results warrant further interface development, as recommended in Section 7.

2. Related work

Steering assistance has been implemented in production automobiles in the form of power steering systems (Shimizu and Tokunaga, 2015). Power steering relies on a control scheme in which the driver rotates the steering wheel with assistive torque from the power steering system (Takada *et al.*, 2013). Some vehicles use electric power steering (EPS), whereas other vehicles use an alternative form of steering assistance called "active front steering" (AFS) that automatically decreases the steering ratio when vehicle speed decreases[1][2][3] (Kumar, 2012; Li *et al.*, 2014). Both EPS and AFS have been developed to improve steering portability at low speeds.

The development of automated driving systems has expanded the design direction of steering assistance to vehicle safety (Chan, 2017). Until the present decade, steering assistance as a collision avoidance technology was investigated but not featured in production automobiles (Dang *et al.*, 2012). Nevertheless, research has led to some advanced driver assistance systems that can be classified by the level of automation as driver-initiated evasion assistance, corrective evasion assistance and automatic evasion assistance (Dang *et al.*, 2012). Driver-initiated evasion assistance systems use sensors such as cameras or radars to detect road obstacles ahead of a vehicle. A driver indicates the intent to avoid a road obstacle through steering wheel movements that are recognized by the steering assistance system. Support is then provided by a steering actuator that applies torque to the steering wheel to guide the driver around the obstacle. On the other hand, corrective evasion assistance directly initiates steering in situations where braking will not prevent collision. Automatic evasion assistance is the most automated system because it directly initiates steering maneuvers in accordance with various collision avoidance scenarios.

Aside from collision avoidance steering systems, nonemergency steering assistance has been featured on production vehicles to optimize lane-keeping and path-following accuracy. The Nissan ProPILOT Assist is one example that provides small steering corrections to improve lane-keeping on highways[4]. Turn Assist is another type of steering assistance that supports path-following along off-road trajectories with small turning radii[5].

In contrast to past technologies such as AFS, driver-initiated evasion assistance and Turn Assist, the steering assistance interface in the current study allows the driver to directly initiate a turn without holding the steering wheel. The sEMG signals generated from the electrical muscle activity of the driver are converted by the vehicle computer into control signals for a steering motor that is connected to the steering wheel (Figure 1). Consequently, the steering wheel is rotated at a constant SWR. The steering wheel could be mechanically linked to the front wheels through a steering column or through a steer-by-wire connection that relies on the vehicle computer to convert steering wheel rotation into electric actuator signals that steer the road wheels (Ackermann, 1997).

Biceps brachii sEMG signals from the right arm execute rightward turning maneuvers, whereas the sEMG from the biceps brachii of the left arm executes leftward turning maneuvers. Surface electrodes that sense these signals and the equipment that converts the signals into steering wheel rotation constitute the human–machine interface (HMI) of the steering assistance system (Figure 1). HMIs enable interactions between humans and machines. Examples include computers that allow operators to control machining devices and equipment for offshore drilling (Martinsen *et al.*, 2016; Strand and Lundteigen, 2017). Other interfaces allow sEMG to control prosthetic limbs and other devices (Basmajian and De Luca, 1985; Hakonen *et al.*, 2015). HMIs involving gestures that produce sEMG signals have been investigated for the purpose of navigating computer screen icons, inputting keyboard commands and controlling a robotic arm (Nagata *et al.*, 2007; Tuisku *et al.*, 2012). The existence of these interfaces indicates that sEMG is a versatile HMI technology.

HMIs that use sEMG have been proposed for controlling different types of vehicles. Facial gestures produce myoelectric signals that enable people to control wheelchairs (Felzer and Freisleben, 2002; Rivera and Desouza, 2012). Myoelectric signals from hand gestures have been used to control a model military tank (Takizawa *et al.*, 2009). Despite the existence of various sEMG controlled devices, there are only a few studies related to sEMG controlled automobiles (Kwak *et al.*, 2008; Nacpil *et al.*, 2018). The current study advances the application of sEMG to automotive control systems by investigating a sEMG controlled steering assistance interface.

3. Design of the steering assistance system

One design objective of the steering assistance system is to enable hands-free steering wheel rotation to prevent decreased steering portability when a vehicle travels at low speeds of 30 km/h or less or at parking speeds near or equal to 0 km/h (Dinh and Kubota, 2013; Sharp and Granger, 2003). Hands-free rotation also meets the design objective to reduce the risk of

Figure 1 Overall steering assistance control design

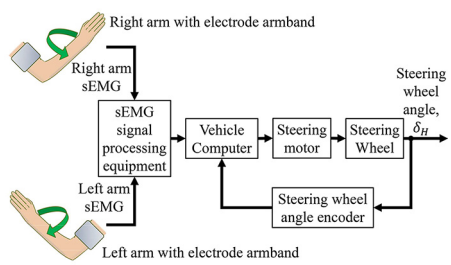

shoulder injury resulting from rapid two-handed steering (Pandis *et al.*, 2015).

Considerations regarding the control design and operation of the steering assistance interface are provided in Section 3.1. Although the steering assistance system was intended for an actual automobile, path-following accuracy was validated with a driving simulator for the safety of the test subjects and to identify how the interface could be improved prior to further development. The adaptation of the interface to a driving simulator is discussed in Section 3.2.

3.1 The steering assistance interface

Consideration was given to the possible ways in which myoelectric signals could be measured. There are multiple gestures with corresponding sEMG signals that could be assigned to steering maneuvers (Nacpil *et al.*, 2018). In a previous study, a radio-controlled model vehicle was successfully steered to the right by supinating the right forearm (Takizawa *et al.*, 2009). Because the biceps brachii is one of the most active muscles when the forearm supinates with the elbow flexed at 90°, the sEMG of the biceps brachii was selected to readily control the steering wheel angle (SWA) of the simulated vehicle (Bader *et al.*, 2018).

If the proposed steering assistance system were to be implemented in an actual automobile, the steering control system design would use sEMG data acquisition equipment, as shown in Figure 1. Gesture-sensing technology that is functionally similar to commercially available technologies, such as the Myo Armband, would be worn on the left and right arms of the driver and would consist of dry electrodes that sense sEMG signals from the biceps brachii muscles[6]. Twisting the forearms through supination produces biceps brachii sEMG signals that are wirelessly transmitted by the armbands to signal processing equipment so that the signals are rectified and averaged. The signals are then converted to steering motor commands by the onboard vehicle computer.

For a steer-by-wire system, hydraulic power assistance at low vehicle speeds enables the steering motor to meet the increased steering torque demand at the front road wheels (Yih and Gerdes, 2005). If the steering wheel is mechanically linked to the road wheels with a steering column, some commercially available steering motors can meet the increased demand for torque by providing more steering wheel torque than human drivers (Forkenbrock and Elsasser, 2005; Sharp and Granger, 2003). Whether a mechanical or steer-by-wire connection is implemented, the SWA resulting from the steering motor would be relayed by an encoder to the vehicle computer so that steering motor commands are adjusted with respect to the measured SWA.

The flowchart in Figure 2 provides an overview of the operation scheme for the proposed steering assistance interface. Vehicle automation used by this scheme falls along a spectrum that ranges from Levels 0 to 5 (*J3016*, 2014). Level 0 automation requires the driver to perform all aspects of the dynamic driving task, i.e. acceleration, braking, steering and monitoring of the vehicle and roadway, whereas a vehicle with Level 5 automation performs the dynamic driving task without a driver. Because automobiles with Levels 4-5 technology can steer automatically, the proposed steering assistance would be redundant for these vehicles. In contrast, Levels 1-3

Figure 2 Operation scheme of steering assistance interface

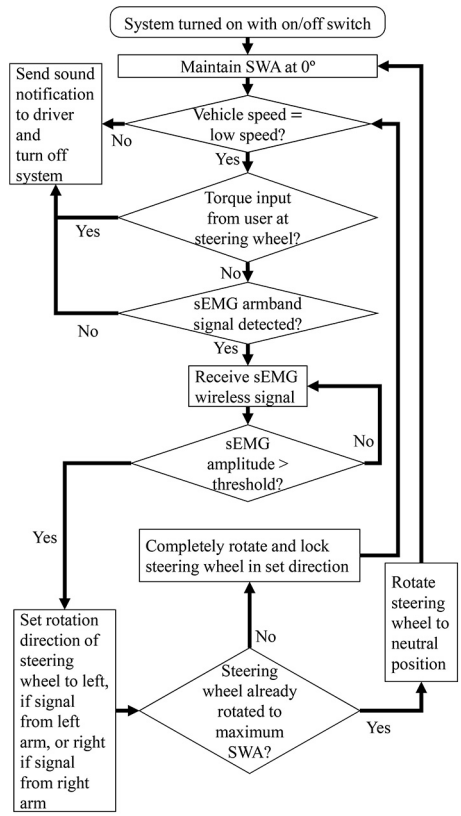

automation allows the driver and the vehicle to have shared control over steering. The current operation scheme applies to this range of automation, as the driver shares control with the steering assistance system.

The relation between the sEMG input of the driver and the rotational output of the steering wheel depends on the SWA that is conventionally represented as δ_H (ISO 4138:2012(E), 2012). If the steering wheel is at the neutral position, supination of the left forearm results in leftward steering wheel rotation until the maximum leftward SWA is reached (Figure 3). On the other hand, supination of the right arm results in rightward steering wheel rotation up to the maximum rightward SWA.

The steering assistance system uses a finite state machine (FSM) control scheme that converts sEMG input to the rotational output of the steering wheel (Figure 3). As in the case of past applications of FSM, such as prosthetic hands and power wheel chairs, the movement of the plant, i.e. the steering wheel, is divided into the following states:

- maximum leftward SWA, $-\delta_{Hmax}$;
- maximum rightward SWA, $+\delta_{Hmax}$; and
- the neutral position, where δ_H is 0° (Cipriani *et al.*, 2008; Felzer and Freisleben, 2002; Geethanjali, 2016).

If the amplitude of the average rectified sEMG from the driver exceeds a specified threshold, e.g. 30 per cent of the signal peak that is determined during the calibration of the sEMG armband to the driver, the vehicle computer determines which arm generated the sEMG signal (Figure 2). Based on the current SWA of the steering wheel, the vehicle computer then changes

Figure 3 Relation between sEMG input and rotational output of steering wheel

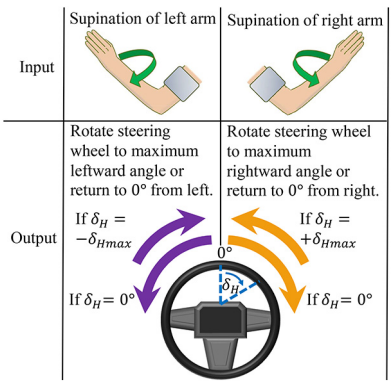

the state of the steering wheel by sending a command to the steering motor.

Visual feedback is provided by the position of the driver relative to the surroundings of the vehicle (Land and Horwood, 1995; Land and Lee, 1994). When performing turns with small radii of curvature, for example, visual feedback from the road is used to maintain lateral distance between the driver and the lane marking of a curve (Land and Lee, 1994). Because this visual feedback is available in the simulated driving scenarios of the current study, other methods of steering feedback, such as vibrotactile devices, are not incorporated into the design of the steering assistance interface (Manawadu *et al.*, 2017).

Because the proposed steering assistance is intended for controlling steering wheel states at low speed or parking speed, the maximum vehicle speed at which states can transition or be maintained without losing steering control is determined through simulation or actual vehicle testing (ISO 4138:2012 (E), 2012; Renfroe *et al.*, 2007; Tandy *et al.*, 2015). As a safety measure, if the maximum speed is exceeded when the steering assistance system is on, a sound notification is sent to the driver, such as a tone lasting several seconds so that the driver can resume manual control of the steering wheel (Figure 2). Note that the same notification would be sent if no signal is provided from the armband.

Before the steering assistance system is turned on, the driver confirms that the SWA is at or close to 0° and the vehicle is stationary. Thus, it would not be recommended to turn on the system in emergency situations, such as the instant before a collision, where there is no time to stop the vehicle and move the steering wheel toward the neutral position. When steering assistance is turned on, the driver lets go of the steering wheel so that the vehicle computer maintains the SWA at 0° (Figure 2). The driver could then supinate the forearms to rotate the steering wheel (Figure 3).

During the operation of the interface, there is a possibility that arm gestures intended for other tasks, such as the operation of the stereo, may produce sEMG signals that would inadvertently cause steering wheel rotation. Therefore, when the driver wishes to preform another task besides the rotation of the steering wheel, steering assistance can be deactivated by pressing an on/off switch at a convenient location such as the dashboard.

While steering assistance is active, the driver may suddenly need to control the steering wheel manually, as in the case where a collision avoidance task cannot be sufficiently addressed by the steering assistance system. Therefore, as a safety precaution, a torque sensor that is similar in function those found on production vehicles would be installed in the steering wheel to allow the driver resume manual control through torque input[4] (Figure 2). A sound notification lasting several seconds would then inform the driver that steering assistance has been deactivated. Note that sound notification and torque sensing were not included in the current study because the simulated driving scenarios did not involve manual takeover.

Efficiently addressing the possibility that the driver would suddenly resume manual control is one way in which the sEMG-based interface is superior to some hands-on interfaces. Joysticks have been developed, for example, as alternatives to the steering wheel for people without health conditions and those with disability (Gil *et al.*, 2013; Manawadu *et al.*, 2017). As a possible interface for the steering assistance system, a joystick may be installed at a vehicle cabin location such as the center console if there is no space that is adjacent to the steering wheel (Wada and Kameda, 2009). When the driver resumes manual control of the steering wheel to avoid a collision, the hand of the driver requires time to traverse the distance between the steering wheel and the joystick. However, the hand would traverse a shorter distance during the operation of the sEMG-based interface as along as the hands of the driver are closer the steering wheel than the possible location of a joystick. Users could be trained to hold their hands close to the steering wheel without interfering with its automatic rotation.

Other alternative interfaces that rely on motion tracking devices, such as the leap motion controller, can detect gestures such as forearm supination, thereby providing hands-free steering wheel rotation (Akyol and Canzler, 2000; Chandarana *et al.*, 2017). As in the case of joysticks, however, the sensor for the motion tracking device may be installed in a location that adds more distance between the hands of the driver and the steering wheel, in comparison to the sEMG-based interface.

This problem could be avoided with accelerometers that measure forearm supination because the hands could be held close to the steering wheel. Nevertheless, accelerometry is subject to noise from vehicle vibrations and unintentional driver movement (Pradko and Lee, 1969). Whether the frame of reference for an accelerometer is located inside or outside of the vehicle, relative movement between the frame of reference and the accelerometer caused by vehicle acceleration could be a source of considerable noise that would render accelerometry impractical.

Unlike accelerometers, electroencephalogram (EEG) signals from the brain do not rely on a kinematic frame of reference. However, an EEG-based brain–computer interface (BCI) would be subject to noise, in addition to BCI illiteracy that affects about 20 per cent of users (Lotte *et al.*, 2013; Minguillon *et al.*, 2017). "BCI illiteracy" refers to low user performance and the inability to operate BCIs that prevented a driver in one study from steering a farm tractor with EEG signals (Gomez-Gil *et al.*, 2011). The neuroheadset that measured the EEG was repurposed so that the driver was able to steer the tractor with

sEMG signals from the scalp. The sEMG-based interface was almost as accurate as the tractor steering wheel with respect to path-following.

Although sEMG technology is subject to its own set of potential problems, including electromagnetic interference, the use of signal filtering, bipolar electrodes and wireless sEMG signal transmission can mitigate some of the interference (Hakonen *et al.*, 2015; Merletti *et al.*, 2009). Further precautions such as an on/off switch and a torque sensor in the steering wheel for manual takeover are incorporated into the steering assistance system (Figure 2). By considering the advantages and disadvantages of various prospective interfaces, the sEMG-based interface has been selected to control the steering assistance system.

3.2 Adaptation to a driving simulator

The sEMG-based HMI was adapted to a driving simulator with a focus on ease of implementation (Figure 4). Components that comprise the sEMG acquisition equipment of the interface were chosen on the basis of affordability and, in cases where the components had to be designed and constructed, component complexity was minimized. Such a strategy was appropriate because the objective of the experiment was the validation of path-following accuracy rather than the complete implementation and testing of all HMI components.

An armband consisting of electrodes was to serve as the sEMG-based HMI for an actual automobile (Section 3.1). However, before investing time and effort in the development of the armband, a readily available and affordable substitute for the armband was used. Disposable Ag/AgCL bipolar electrodes were attached to the biceps brachii longhead, and a ground electrode was mounted on the wrist in accordance with the recommendations of SENIAM (Surface EMG for the Non-Invasive Assessment of Muscles) (Hermens and Freriks, 1997). Because the lateral portion of the biceps brachii belly provided a peak signal with the least variability in comparison to the medial and central portions, bipolar electrodes were placed along the lateral portion (Mercer *et al.*, 2006). Bipolar electrodes were selected because they were more resistant to noise than other sensors such as monopolar electrodes (Hakonen *et al.*, 2015).

Given that one design objective of the steering assistance system is to reduce the risk of shoulder injury to the driver during sudden two-handed rotation of the steering wheel to the right, all the simulated driving scenarios involved the rapid execution of rightward turning maneuvers (Figure 5) (Pandis *et al.*, 2015). Consequently, only sEMG input from the right arm was used because the right arm exclusively controlled rightward steering (Figure 3).

In previous studies involving males and females, the median electromyography reaction time for the sEMG signal of the right arm biceps brachii was faster than that of the left arm by 3-4 per cent (Nakamura and Saito, 1974; Nakamura and Taniguchi, 1980). Because supination of the left arm rather than the right arm would add a negligible increase to the steering response time, it was expected that there would be a correspondingly negligible effect on path-following accuracy. Therefore, performing turns with the right arm alone was sufficient for path-following validation.

A custom sEMG data acquisition device (DAQ) was developed for the sEMG-based HMI (Figure 6). Control signals were processed with the DAQ and a Windows 10 platform laptop. (Panasonic CF-LX6 laptop with a 14-inch, 1920 × 1080 resolution screen.) The DAQ consisted of a custom circuit that applied filtering so that only analog signals with frequencies ranging from 2 to 530 Hz were amplified with a gain of 5,000. Amplified analog signals were digitized with a sampling rate of 10 kHz. The digital signals were rectified before applying a moving average with a window size of 50 data points. Then the signals were mapped onto an analog joystick control scheme with a sEMG amplitude of 0 corresponding to a centered joystick position and the peak amplitude corresponding to the maximum rightward joystick position. Because the driving simulator accepted keyboard commands, the laptop executed software to convert joystick commands into keyboard commands so that the steering of the driving simulator, Digital Battlespace 2™ (DBS2™, Bohemia Interactive), could be controlled. Whenever a test subject initially connected or reconnected to the DAQ, calibration of the DAQ was performed by using the game controller calibration software included with Windows 10. Based on this calibration, the threshold for sEMG control signals was set from 10 to 30 per cent of the peak signal resulting from forearm supination lasting up to 1 s. This setting prevented the detection of inadvertent sEMG signals and other interferences below the threshold.

As the test subjects operated the sEMG-based HMI, acceleration and braking were controlled with a set of foot pedals that originally came with the commercially available game steering wheel (Driving Force™ GT). The game steering wheel had force feedback and a steering ratio of 1:1 (Figure 7). As the steering of the driving simulator could be controlled without input from the game steering wheel, sEMG input controlled the steering in the simulator rather than the rotation of the game steering wheel.

In addition to using the steering assistance interface to complete the driving scenarios, the test subjects repeated the scenarios with the game steering wheel as a basis for comparison.

Figure 4 Steering assistance interface for driving simulator

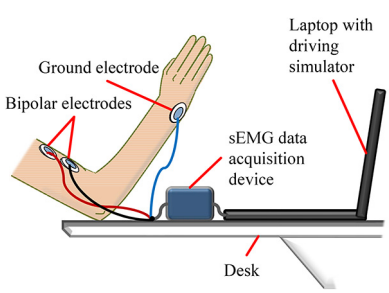

4. Experimental methodology

The objective of the experiment was to validate the path-following accuracy of the sEMG-controlled interface with a

Figure 5 Three driving simulator scenarios

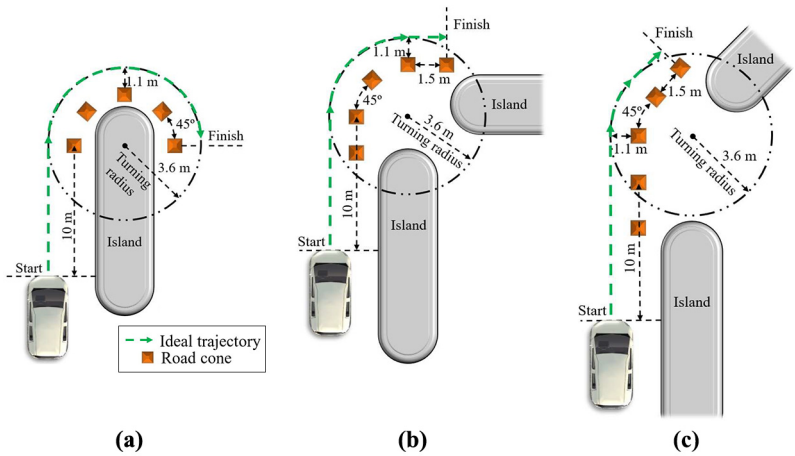

(a) **(b)** **(c)**

Notes: (a) U-turn; (b) 90° turn; (c) 45° turn

Figure 6 Steering control system for driving simulator

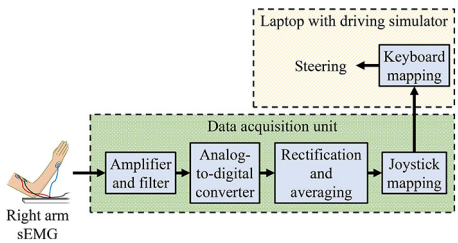

Figure 7 Experimental setup

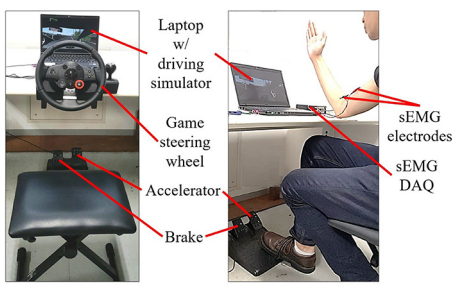

(a) **(b)**

Notes: (a) Game steering wheel; (b) steering assistance interface

driving simulator. If the use of the interface was associated with a path-following accuracy that was at least comparable to the use of the game steering wheel, then the sEMG-based HMI would be successfully validated.

Driving scenarios that were simulated in the experiment were constructed to test the interface with rapid SWRs at vehicle speeds below 30 km/h. The design of the scenarios and a general strategy for completing the scenarios with maximized path-following accuracy are detailed in Section 4.1. An experimental protocol for validating path-following accuracy is provided in Section 4.2.

4.1 Driving scenarios

As the steering assistance system was designed to reduce the risk of shoulder injuries posed by rapidly rotating the steering wheel to the right from 0° to 65°, all the simulated driving scenarios were designed to necessitate rapid SWRs and steering wheel rotation up to 65° to maximize path-following accuracy (Pandis *et al.*, 2015). As a means of ensuring that this SWA would be necessary, the ideal trajectory in each scenario had a radius of curvature corresponding to the SWA. Given that the SWA corresponded to the smallest turning radius of the virtual car, the test subjects were instructed to only rotate the steering wheel up to the SWA. On the other hand, when test subjects used the sEMG-based interface, the virtual car would be steered to the turning radius at a constant SWR.

The need to rapidly rotate the steering wheel to optimize path-following accuracy was determined by the driving scenarios. Distance was allotted between the starting line in each scenario and the cone at the beginning of each turn (Figure 5). Test subjects were instructed to accelerate from the start line without braking or decelerating so that the speed at the beginning of the turn was nonzero. Because the ideal trajectory of the turn in each scenario had a radius of curvature equal to the smallest turning radius of the virtual car, it was possible to optimize path-following accuracy, if the steer angle of the road wheels corresponded to the smallest turning radius.

This steer angle, i.e. the Ackermann steer angle, is a vehicle characteristic that applies to steady-state turning, where speed, SWA and the smallest turning radius are constant (ISO 4138:2012(E), 2012; Tandy *et al.*, 2015). There is a transient phase prior to this steady-state in which the steering wheel rotates from the neutral position to 65°. A briefer transient phase entails that the Ackermann steer angle can be attained in less time. Therefore, the SWRs of the game steering wheel and the sEMG-based interface could be maximized to reduce the transient phase and to optimize path-following accuracy.

Aside from the Ackermann angle, a vehicle characteristic that is relevant to path-following is the steering-wheel angle gradient (ISO 4138:2012(E), 2012):

$$steering\text{-}wheel\ angle\ gradient = \frac{\partial \delta_H}{\partial a_Y} \quad (1)$$

A vehicle that follows a circular path at increasing speed generates centrifugal force on the vehicle that alters the turning circle and increases the lateral acceleration, a_Y, away from the center of the turning circle. Consequently, the SWA, δ_H, is adjusted to maintain a circular path. The changes in SWA and lateral acceleration constitute the steering-wheel angle gradient expressed by Equation (1).

This equation is modified to account for two steering phenomena that affect path-following accuracy, namely, oversteer and understeer. Dividing Equation (1) by the steering ratio of the vehicle yields the understeer gradient (ISO 4138:2012(E), 2012):

$$understeer\ gradient = \frac{\partial \delta_H}{\partial a_Y} \times \frac{1}{i_S} \quad (2)$$

The steering wheel ratio, i_S, for the game steering wheel is 1:1, and therefore Equation (2) reduces to Equation (1).

Understeer can occur when the radius of the circular path increases because of increasing lateral acceleration, a_Y. Because empirical testing demonstrates that δ_H and a_Y are positively associated, the driver should increase δ_H in the direction of the turn to correct for understeer and to restore steady-state steering (Tandy *et al.*, 2015). On the other hand, oversteer can occur when the radius of the circular path decreases because of decreasing lateral acceleration. Thus, δ_H is decreased by the driver in accordance with Equation (2) to restore steady-state steering. Whereas Equation (2) applies to the game steering wheel, the understeer gradient is modified to apply to the sEMG-based interface. As the steering assistance system maintains a constant SWA during steady-state steering, the understeer gradient becomes (ISO 4138:2012(E), 2012):

$$understeer\ gradient = l \times \frac{\partial \frac{1}{R}}{\partial a_Y} \quad (3)$$

The understeer gradient is determined by the length of the vehicle, l, lateral acceleration, a_Y, and the radius of curvature, R, of the circular path. Because empirical data typically indicate a negative association between$1/R$ and a_Y, a decrease in a_Y results in an increase in $1/R$ and thus a decrease in R (Tandy *et al.*, 2015). In the case of oversteer, the decrease in R can be mitigated by pressing the accelerator to increase lateral acceleration, a_Y. As understeer increases R, the driver corrects by releasing the accelerator or braking to decrease lateral acceleration. In summary, even though the steering wheel is held at a fixed angle, the driver could correct understeer and oversteer by longitudinally decelerating or accelerating the vehicle, respectively.

Based on transient and steady-state steering, a general strategy can be devised to maximize path-following accuracy for the driving scenarios (Figure 5). As mentioned previously in this section, there is a transient phase at the beginning of a turn involving the steering of the front road wheels to the Ackermann steer angle. When steady-state steering begins, the game steering wheel or, in the case of the sEMG-based interface, the accelerator can be adjusted to correct oversteer and understeer. Hence, the general strategy can be executed in the following sequence:

1 Maintain a constant low speed before and throughout the turn to prevent oversteer and understeer. This can be accomplished by constantly pressing the accelerator and not pressing the brake before and during the turn.
2 At the beginning of the turn, rotate the game steering wheel to 65° as soon as possible, or in the case of the sEMG-interface, supinate the right arm as soon as possible.
3 If oversteer should occur during the turn, rotate the steering wheel to the left, if applicable, or press the accelerator further.
4 If understeer should occur during the turn, rotate the steering wheel to the right, if applicable, or reduce accelerator depression. If the steering wheel is already rotated to the maximum SWA of 65°, understeer cannot be corrected with the steering wheel.
5 Do not return the vehicle to a longitudinal trajectory until the vehicle reaches the last road cone along the ideal circular trajectory.

Notice that item (1) in the above strategy is based on observations related to Equation (2), whereas item (2) is related to the previous discussion in this section regarding the minimization of the transient steering phase of a turn. Items (3) and (4) are based on observations regarding Equations (2) and (3). Finally, following item (5) maintains steady-state steering throughout the turn so that path-following accuracy can be maximized as mentioned previously in this section.

Items (1)-(5) were demonstrated through training videos for drivers who participated in experimental trials.

4.2 Experimental procedure

Experimental trials with the driving simulator were completed by a group of 24 healthy drivers, consisting of two females and 22 males. One test subject was left-handed and the rest were right-handed. The ages of test subjects ranged from 20 to 45 years, with an average age of 23. Thirteen test subjects had previous driving simulator experience. All test subjects had between six months and seven years of driving experience, and the test subjects all had standard driver's licenses issued by the Government of Japan. The test subjects were recruited through referrals from colleagues at The University of Tokyo and by response to recruitment flyers that were posted on the university campuses. Ethical approval for this experiment was obtained from the ethics committee of the Interfaculty Initiative in Information Studies within the Graduate School of Interdisciplinary Information Studies at The University of Tokyo.

Test subjects completed driving scenarios with the sEMG-based HMI and the game steering wheel (Figure 5). Acceleration and braking of the car were performed with a set of pedals. A turning maneuver was completed only if the center of the front bumper of the car passed the first and last road cones along the turn without running into an island. Furthermore, the test subjects were instructed not to press the brake pedal until the car cleared the last road cone so that the execution of a turn would not be influenced by the operation of the brake pedal. However, releasing the accelerator was

allowed, as this operation was included in the strategy outlined in Section 4.1.

Operation of the sEMG-based HMI followed the steps shown in Figure 8. First, the accelerator was pressed to move the virtual car forward, and then the test subject supinated the right forearm to begin turning to the right. The test subject then supinated the right forearm again to exit the right turn before pressing the brake pedal to stop the virtual car. The same procedural structure was repeated with the game steering wheel in place of the sEMG-based HMI.

Figure 8 sEMG-based HMI operation sequence

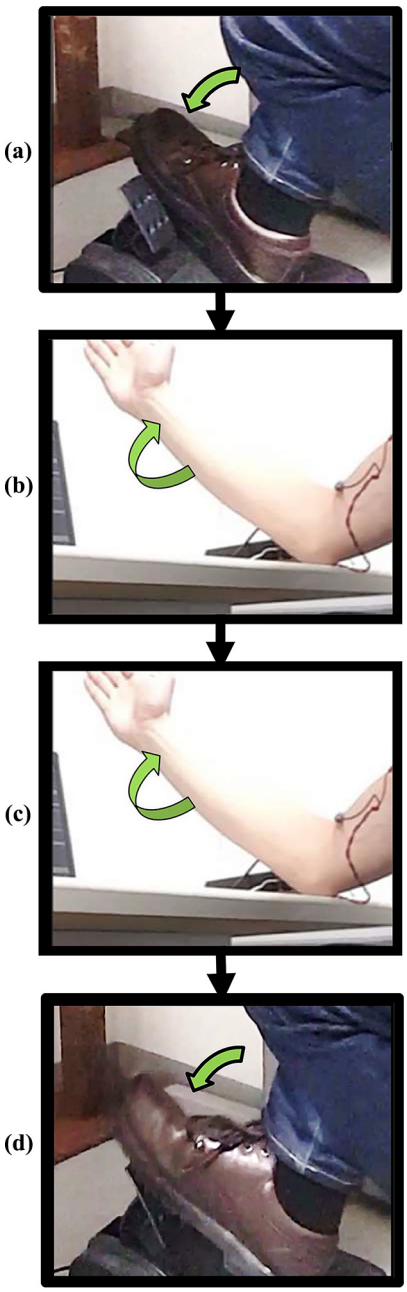

Notes: (a) Press accelerator; (b) supinate right arm to initiate turn; (c) supinate right arm to terminate turn; (d) press brake

Throughout the execution of a right turn, the elbow of the test subject rested on a desk (Figure 8). This assisted with the maintenance of elbow flexion at 90° and flexion of the right arm at 90° from the anatomical position. When the virtual car was not turning, the surface of the palm of the right hand was held nearly parallel to the sagittal plane. Given that the virtual car was moving forward along a linear trajectory, supination of the right forearm steered the front road wheels of the virtual car to the rightward Ackermann steer angle. Supinating the forearm again returned the front wheels to their original positions so that the virtual car could continue moving forward along a linear trajectory.

Training of the test subjects involved the viewing of a slide presentation that included written interface operation instructions as well as videos of an expert user demonstrating the operation of each interface for each driving scenario. Test subjects who viewed the presentation went on to complete driving simulator training for the sEMG interface equipment, followed by driving simulator training for the game steering wheel. Training for a given interface consisted of the completion of driving scenarios in the following order: U-turn, 90° turn and 45° turn (Figure 5). Each scenario had to be successfully completed twice before a test subject could move on to the driving simulator trials for data collection.

Two simulated SWR settings for the sEMG-based HMI were used during the experimental trials to observe the effect SWR on path-following accuracy. Some commercially available steering motors could provide maximum SWRs that ranged from 720 to 1,300 deg/s (Forkenbrock and Elsasser, 2005). However, the driving simulator was only capable of providing a maximum simulated SWR of 720 deg/s. Given that all the driving scenarios were designed to require the SWA to transition between 0° and 65°, the transient steering phase was determined by dividing 65° by 720 deg/s to get 0.1 s. This was the transient phase of the *fast-turning sEMG-based HMI*. A considerably longer transient phase of 1 s for the *slow-turning sEMG-based HMI* was also tested to confirm an *a priori* observation derived from the discussion in Section 4.1 – that prolonging the transient phase reduces path-following accuracy. According to this observation, the fast-turning interface would be more accurate than the slow-turning interface. Furthermore, as previous driving simulator testing has shown that the transient phase for two-handed steering wheel rotation was 0.268 SD 0.065 s, the fast-turning interface would be more accurate than the game steering wheel, whereas the slow-turning interface would be less accurate (Pandis *et al.*, 2015). Hence, it was anticipated that the experiment would confirm the following:

H1. For most of the tested driving scenarios, the slow-turning sEMG-based HMI has a lower path-following accuracy than the game steering wheel.

H2. For most of the tested driving scenarios, the fast-turning sEMG-based HMI has a higher path-following accuracy than the game steering wheel.

The experiment was structured to test these hypotheses by evenly dividing the test subjects into two groups, shown in Table I. Group A consisted of 12 test subjects who completed the three driving scenarios in Figure 5 with the game steering wheel and the fast-turning sEMG-based interface. Therefore, each member of Group A participated in a total of six experimental conditions that are listed as 1-6 in Table I. Conditions 1-3 were compared to conditions 4-6, respectively, to assess *H2*. Group B consisted of another 12 test subjects who followed the same procedure as Group A, but the slow-turning sEMG-based interface was used instead of the fast-turning counterpart. Each member of Group B participated in another set of six experimental conditions that are listed as 7-12 in Table I. Conditions 7-9 were compared to conditions 10-12, respectively, to assess *H1*.

Within-subject randomization for the conditions of Group A was carried out by dividing the group into two subgroups of six and applying a balanced 6 × 6 Latin square to each subgroup (Shuttleworth, 2009). The same randomization was applied to the conditions of Group B.

Each test subject was allowed five attempts per condition. Given that thee sEMG-based HMIs fell under the category of sEMG interfaces and the game steering wheel fell under the category of steering wheel interfaces, the number of experimental trials was calculated as follows:

$$3\ \textit{driving scenarios} \times 5\ \textit{attempts} \times 24\ \textit{test subjects} \times 2\ \textit{interface categories} = 720\ \textit{trials} \tag{4}$$

As a means of reducing the risk of insufficient data from each test subject, only the first three successful attempts for each experimental condition were used for data analysis.

The shortest distance between the ideal trajectory and the edge of a given road cone in any attempted scenario was 1.1 m (Figure 5). The lateral error of the actual trajectory was calculated by finding the absolute value of the difference between 1.1 m and the shortest distance between the actual trajectory and the edge of the road cone. Because there are five cones per scenario, the lateral error was calculated five times for each trial. For each condition in Table I, the median lateral error was calculated across trials. The data spread about the median lateral error was expressed as the interquartile range (IQR) (Upton and Cook, 1996).

Data used to calculate path-following accuracy were also used to generate two-dimensional plots of the median trajectories for each interface. Data from Group A and Group B were used to plot the median trajectories for the fast- and slow-turning sEMG interfaces, respectively. The median trajectory for the game steering wheel was plotted from the data of both groups. Observations were made from the driving trajectories regarding the relation between the driving scenarios and path-following accuracy (Section 5).

Statistical significance tests were the criteria for confirming *H1* and *H2*. Some data sets did not have a normal distribution as indicated by Shapiro–Wilk tests, where $p < 0.05$ (Shapiro and Wilk, 1965). Thus, the nonparametric Wilcoxon signed-rank test was used to calculate statistical significance with a significance level of $p < 0.05$ (Whitley and Ball, 2002). If there was a statistically significant difference in the sense that the game steering wheel had higher path-following accuracy than the slow-turning sEMG-based HMI for most of the tested driving scenarios, then *H1* would be confirmed. Similarly, *H2* would be confirmed if the fast-turning sEMG-based HMI had a lower median lateral error than the game steering wheel, and this difference was statistically significant for most of the tested driving scenarios. Even if *H2* was not confirmed, the path-following accuracy of the steering assistance system would be validated if there was at least no statistically significant difference between the game steering wheel and the fast-turning sEMG based interface.

5. Results and discussion

Based on data from the experimental trials, the path-following accuracy of a simulated automobile was calculated for a U-turn, 90° turn and 45° turn (Figure 5). Drivers in Group B used the game steering wheel and the slow-turning sEMG-based HMI to complete the scenarios (Table I). The results for Group B showed a statistically significant difference, namely, that the slow-turning sEMG-based HMI was significantly less accurate than the game steering wheel when performing a U-turn [Figure 9(b)]. There was no significant difference, however, in the case of the 90° and the 45° turns. Therefore, *H1* was rejected because the sEMG-based HMI was comparable to the game steering wheel in most of the scenarios (Section 4.2).

Drivers in Group A completed the driving scenarios with the game steering wheel and the fast-turning sEMG-based HMI (Table I). The drivers steered with greater accuracy in all scenarios with the fast-turning sEMG-based HMI than with the game steering wheel [Figure 9(a)]. Because the U-turn was the only scenario where the difference between the interfaces was statistically significant, *H2* was rejected (Section 4.2). Nevertheless, the fast-turning sEMG interface was at least comparable to the game steering wheel across all tested scenarios, and therefore the path-following accuracy of the fast-turning sEMG interface was validated.

Path-following accuracy varies between trials as indicated by the data summary in Table II. The IQR values for the slow-turning sEMG-based HMI are all higher than those of the other

Table I Experimental conditions

Test subject group	sEMG-based interface type	sEMG-based interface conditions	Game steering wheel conditions
Group A	Fast-turning	Condition 1: U-turn	Condition 4: U-turn
		Condition 2: 90° turn	Condition 5: 90° turn
		Condition 3: 45° turn	Condition 6: 45° turn
Group B	Slow-turning	Condition 7: U-turn	Condition 10: U-turn
		Condition 8: 90° turn	Condition 11: 90° turn
		Condition 9: 45° turn	Condition 12: 45° turn

Figure 9 Comparison of steering interfaces with respect to median lateral error

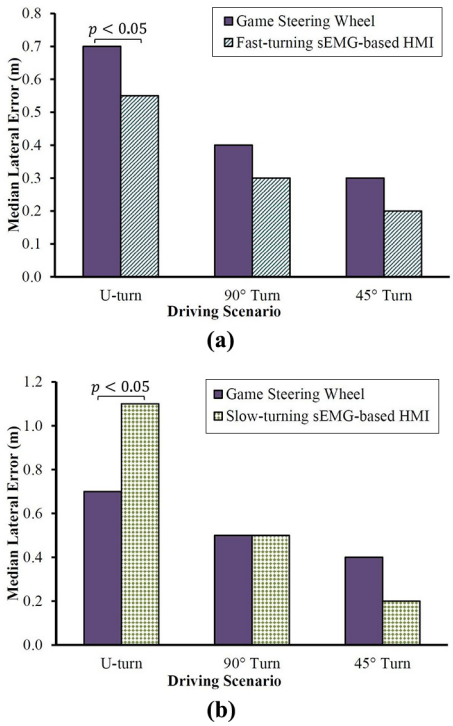

interfaces, meaning that the accuracy of the slow-turning sEMG-based HMI has the highest variability. In contrast to the other interfaces, the accuracy of the fast-turning sEMG-based HMI varies the least with IQRs that are consistently low across all scenarios. The fast-turning sEMG-based HMI is therefore associated with more repeatable path-following.

One pattern that is associated with all the interfaces, is the decrease in the median lateral error as the angle of the turning maneuver decreases from the U-turn angle to 45° (Table II). A possible reason for this pattern pertains to the median trajectories shown in Figure 10. The U-turn trajectories for all interfaces have the lowest error at the first road cone along the ideal trajectory because the longitudinal trajectory of the simulated car at the beginning of the scenario is enough to follow the ideal trajectory at the first road cone [Figure 10(a)]. A longitudinal trajectory of the virtual car provides the highest accuracy before reaching the third road cone in the 90° turn and before reaching the fourth road cone in the 45° turn [Figure 10(a) and (b)]. It is therefore expected that driving scenarios involving longer longitudinal trajectories are associated with higher path-following accuracy, as evidenced by Table II. In contrast, scenarios involving longer circular paths are associated with lower path-following accuracy. The median trajectories account for this lower accuracy by indicating that lateral error tends to progressively increase with the length of a turn. Notice that all the median trajectories terminate at the finish lines with lateral distances from the final road cones that are greater than the lateral distances from the initial road cones (Figure 10).

There are potential explanations for the lateral error in Table II. Although it may be a cause of lateral error, understeer does not explain why the median trajectory of the fast-turning sEMG interface tends to be the closest to the ideal trajectory, whereas the median trajectory of the slow-turning sEMG interface tends to be the farthest. Because these two interfaces only differ with respect to the duration of their transient steering phases (Section 4.1), perhaps there is a relation between transient steering phases and lateral errors. As opposed to the 1 s transient steering phase of the slow-turning sEMG interface, the fast-turning sEMG interface has a transient steering phase of 0.1 s. This shorter period allows steady-state steering to begin earlier in the turn, resulting in a median trajectory with higher path-following accuracy. As a previously tested steering wheel for a driving simulator has an intermediate transient time of 0.268 SD 0.065 s, the median trajectory of the game steering wheel in the current study would hypothetically have the second highest path-following accuracy (Pandis *et al.*, 2015). This expectation is confirmed because the median trajectory with the second largest lateral distance from the ideal trajectory tends to belong to the game steering wheel (Figure 10).

Although Figure 10 shows that the median trajectories of the interfaces differ with respect to path-following accuracy, only the U-turn is associated with statistically significant differences between the interfaces (Figure 9). The U-turn thus appears to be the most effective of the simulated scenarios at distinguishing the path-following accuracy of the interfaces.

Table II Summary of path-following accuracy data

Test subject group	Interface type	Driving scenario	Median lateral error (m)	IQR (m)
Group A	Fast-turning sEMG-based HMI	U-turn	0.55	0.8
		90° turn	0.3	0.8
		45° turn	0.2	0.8
	Game steering wheel	U-turn	0.7	0.9
		90° turn	0.4	1
		45° turn	0.3	0.8
Group B	Slow-turning sEMG-based HMI	U-turn	1.1	1.8
		90° turn	0.5	1.4
		45° turn	0.2	1.4
	Game steering wheel	U-turn	0.7	1
		90° turn	0.5	1.2
		45° turn	0.4	1

Figure 10 Median and ideal trajectories

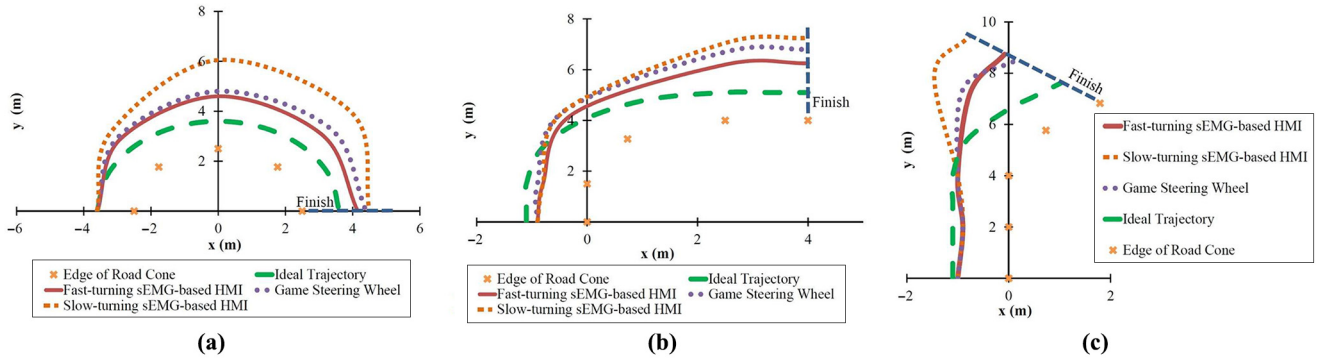

Notes: (a) U-turn; (b) 90° turn; (c) 45° turn

6. Limitations

Given that the average age of the test subjects was 23 years, the results were relevant to regular driver's license holders between the ages of 20 and 24 years, who comprised about 51 per cent of the nearly 9,000,000 regular driver's license holders in Japan as of 2015[7]. Given that some age groups were not represented by the test subjects, the total population of regular driver's license holders in Japan could have been more accurately represented by recruiting a group of test subjects with an age distribution that was close to that of the total population.

Two females and 22 males participated in the experimental trials. Based on data from a previous study that measured the range of motion and velocity of forearm supination, females supinated their left and right forearms 6-8 per cent faster than males, and therfore the results may not have accurately reflected biomechanical differences between males and females (Rahman *et al.*, 2014). Because the the inclusion of more female participants may decrease the median time to perform supinations, and consequently the total time to steer from a lognitudinal trajectory to the turning circle may also decrease, it was expected that the median lateral error of the sEMG-based HMI would decrease, if not remain approximately the same. Thus, the results may have conservatively estimated the accuracy of the sEMG-based HMI.

Setting the SWR of the sEMG-based interface to a transient steering phase of 0.1 s resulted in more accurate U-turns than those of the game steering wheel. As the differences between these interfaces were only statistically significant for the U-turn, further studies that only adjust the SWR could include the U-turn as a driving scenario to observe any statistically significant differences in path-following accuracy. For example, U-turns could be executed to determine different accuracies for transient steering phases between 0.1 s and 1 s. Based on these accuracies, the relationship between path-following accuracy and transient steering phases would be quantified in further detail.

Given that the steering assistance system was validated with a fixed-base driving simulator, steering feedback in the form of lateral vehicle acceleration and other aspects of an actual vehicle environment were not simulated. Furthermore, unlike the virtual car in the driving simulator, actual cars had cornering compliances such as steering system deflections that alter the Ackermann steering angle (ISO 4138:2012(E), 2012). Nevertheless, the design optimization of actual automobile steering systems could minimize the effect of cornering compliances on the Ackermann steering angle, and therefore the results of the current study could closely approximate vehicles with optimized steering systems (Pauwelussen, 2015).

7. Conclusions

An sEMG controlled steering assistance interface with a maximized SWR of 720 deg/s was found to have path-following accuracy that was at least comparable to a game steering wheel. The validation of this accuracy was conducted with a driving simulator that enabled drivers to complete a U-turn, 90° turn and 45° turn. The median lateral errors of the game steering wheel and the sEMG-based HMI indicated that a faster SWR was associated with greater path-following accuracy. The difference in path-following accuracy between the interfaces was statistically significant in the case of the U-turn, with the sEMG-based HMI being more accurate. Thus, future studies could incorporate the U-turn as a means of distinguishing the accuracies of interfaces with varying SWRs.

Acceptable path-following accuracy warrants further development of the sEMG-based HMI for an actual automobile. In place of the wet electrode setup in the current study, a wireless electrode armband consisting of dry electrodes would be configured to provide comparable signal measurement accuracy (Hakonen *et al.*, 2015). In contrast to wet electrodes, dry electrodes do not need conductive electrolyte gel at the skin-electrode interface, and thus drivers would not need to clean the gel after using the electrodes. Another potential improvement would be a vibration device in the wireless sEMG armband to indicate the state of the steering wheel. Other devices could be realized as well, including untested components that were previously proposed, e.g. sound notifications during manual takeover and a motorized steering wheel that can sense torque input from the driver.

Notes

1 https://pressroom.toyota.com/releases/2017-toyota-corolla-product-specs.download

2 https://automobiles.honda.com/images/future-cars/2016-pilot/Pilot_Specs_full.pdf

3 https://automobiles.honda.com/images/2016/accord-sedan/downloads/2016-accord-sedan-specifications.pdf

4 http://nissannews.com/en-US/nissan/usa/releases/nissan-propilot-assist-technology-reduces-the-hassle-of-stop-and-go-highway-driving-ready-for-u-s-launch?la=1&la=1

5 www.toyota.com/content/ebrochure/2018/landcruiser_ebrochure.pdf

6 www.myo.com/

7 www.npa.go.jp/toukei/menkyo/pdf/h26_main.pdf

References

Ackermann, J. (1997), "Robust control prevents car skidding", *IEEE Control Systems Magazine*, Vol. 17 No. 3, pp. 23-31.

Akyol, S. and Canzler, U. (2000), "Gesture control for use in automobiles", *IAPR Workshop on Machine Vision Applications*, *MVA Organization*, *Tokyo*, pp. 349-352.

Bader, J., Boland, M.R., Greybe, D., Nitz, A., Uhl, T. and Pienkowski, D. (2018), "Muscle activity during maximal isometric forearm rotation using a power grip", *Journal of Biomechanics*, Vol. 68, pp. 24-32.

Basmajian, J.V. and De Luca, C.J. (1985), *Muscles Alive: Their Functions Revealed by Electromyography*, in Butler, J. (Ed.), 5th ed., Williams and Wilkins, Baltimore.

Chan, C.Y. (2017), "Advancements, prospects, and impacts of automated driving systems", *International Journal of Transportation Science and Technology*, Vol. 6 No. 3, pp. 208-216.

Chandarana, M., Meszaros, E.L., Trujillo, A. and Allen, B.D. (2017), "'Fly like this ': natural language interfaces for UAV mission planning", *ACHI 2017: The Tenth International Conference on Advances in Computer-Human Interactions*, *IARIA*, *Nice*.

Cipriani, C., Zaccone, F., Micera, S. and Carrozza, M.C. (2008), "On the shared control of an EMG-controlled prosthetic hand: analysis of user-prosthesis interaction", *IEEE Transactions on Robotics*, Vol. 24 No. 1, pp. 170-184.

Dang, T., Desens, J., Franke, U., Gavrila, D., Schäfers, L. and Ziegler, W. (2012), "Steering and evasion assist", in Eskandarian, A. (Ed.), *Handbook of Intelligent Vehicles*, 1st ed., Springer-Verlag, London, pp. 760-782.

Dinh, D.D. and Kubota, H. (2013), "Profile-speed data-based models to estimate operating speeds for urban residential streets with a 30km/h speed limit", *IATSS Research*, Vol. 36 No. 2, pp. 115-122.

Felzer, T. and Freisleben, B. (2002), "HaWCoS: the 'hands-free' wheelchair control system", *ASSETS '02 The 5th ACM SIGCAPH Conference on Assistive Technologies*, *ACM Press*, *Edinburgh*, pp. 127-134.

Forkenbrock, D. and Elsasser, D. (2005), *An Assessment of Human Driver Steering Capability*, National Highway Traffic Safety Administration, Liberty, Washington.

Geethanjali, P. (2016), "Myoelectric control of prosthetic hands: state-of-the-art review", *Medical Devices: Evidence and Research*, Vol. 9, pp. 247-255.

Gil, J.J., Díaz, I., Ciáurriz, P. and Echeverría, M. (2013), "New driving control system with haptic feedback: design and preliminary validation tests", *Transportation Research Part C: Emerging Technologies*, Vol. 33, pp. 22-36.

Gomez-Gil, J., San-Jose-Gonzalez, I., Nicolas-Alonso, L.F. and Alonso-Garcia, S. (2011), "Steering a tractor by means of an EMG-based human-machine interface", *Sensors*, Vol. 11 No. 7, pp. 7110-7126.

Hakonen, M., Piitulainen, H. and Visala, A. (2015), "Current state of digital signal processing in myoelectric interfaces and related applications", *Biomedical Signal Processing and Control*, Vol. 18, pp. 334-359.

Hermens, H. and Freriks, B. (1997), *The State of the Art on Sensors and Sensor Placement Procedures for Surface ElectroMyoGraphy: A Proposal for Sensor Placement Procedures*, SENIAM, Enschede.

ISO 4138:2012(E) (2012), *Passenger Cars – Steady-state Circular Driving Behavior – Open-loop Test Methods*, International Standards Office, Geneva.

J3016 (2014), *Taxonomy and Definitions for Terms Related to On-Road Motor Vehicle Automated Driving Systems*, SAE International, Warrendale.

Kumar, A. (2012), "An overview of active front steering system", *International Journal of Scientific & Engineering Research*, Vol. 3 No. 6, pp. 556-565.

Kwak, J., Jeon, T.W., Park, H., Kim, S. and An, K. (2008), "Development of an EMG-based car interface using artificial neural networks for the physically handicapped", *Korea IT Services Journal*, Vol. 7 No. 2, pp. 149-164.

Land, M. and Horwood, J. (1995), "Which parts of the road guide steering?", *Nature*, Vol. 377 No. 6547, pp. 339-340.

Land, M.F. and Lee, D.N. (1994), "Where we look when we steer", *Nature*, Vol. 369 No. 6483, pp. 742-744.

Li, F., Wang, L., Liao, C. and Wu, Y. (2014), ""Active steering control strategy of steer-by-wire system based on variable steering ratio", *IEEE Transportation Electrification Conference and Expo, ITEC Asia-Pacific 2014 – Conference Proceedings*, *IEEE*, *Beijing*.

Lotte, F., Larrue, F. and Mühl, C. (2013), "Flaws in current human training protocols for spontaneous brain-computer interfaces: lessons learned from instructional design", *Frontiers in Human Neuroscience*, Vol. 7.

Ma, B., Yang, Y., Liu, Y., Ji, X. and Zheng, H. (2016), "Analysis of vehicle static steering torque based on tire-road contact patch sliding model and variable transmission ratio", *Advances in Mechanical Engineering*, Vol. 8 No. 9, pp. 1-11.

Manawadu, U.E., Kamezaki, M., Ishikawa, M., Kawano, T. and Sugano, S. (2017), "A multimodal human-machine interface enabling situation - adaptive control inputs for highly automated vehicles", *2017 IEEE Intelligent Vehicles Symposium (IV)*, *IEEE*, *Los Angeles*.

Martinsen, K., Downey, J. and Baturynska, I. (2016), "Human-machine interface for artificial neural network based machine tool process monitoring", *Procedia CIRP*, *Elsevier B. V.*, *Ischia*, Vol. 41, pp. 933-938.

Mercer, J.A., Bezodis, N., DeLion, D., Zachry, T. and Rubley, M.D. (2006), "EMG sensor location: does it influence the ability to detect differences in muscle contraction conditions?", *Journal of Electromyography and Kinesiology*, Vol. 16 No. 2, pp. 198-204.

Merletti, R., Botter, A., Troiano, A., Merlo, E. and Minetto, M.A. (2009), "Technology and instrumentation for

detection and conditioning of the surface electromyographic signal: State of the art", *Clinical Biomechanics*, Vol. 24 No. 2, pp. 122-134.

Minguillon, J., Lopez-Gordo, M.A. and Pelayo, F. (2017), "Trends in EEG-BCI for daily-life: requirements for artifact removal", *Biomedical Signal Processing and Control*, Vol. 31, pp. 407-418.

Nacpil, E.J., Zheng, R., Kaizuka, T. and Nakano, K. (2018), "Implementation of a sEMG-machine interface for steering a virtual car in a driving simulator", in Cassenti, D.N. (Ed.), *AHFE 2017 International Conference on Human Factors in Simulation and Modeling*, *Springer International Publishing AG*, *Los Angeles*, pp. 274-282.

Nagata, K., Ando, K., Magatani, K. and Yamada, M. (2007), "Development of the hand motion recognition system based on surface EMG using suitable measurement channels for pattern recognition", *2007 29th Annual International Conference of the IEEE Engineering in Medicine and Biology Society, IEEE*, *Lyon*, pp. 5214-5217.

Nakamura, R. and Saito, H. (1974), "Preferred hand and reaction time in different movement patterns", *Perceptual and Motor Skills*, Vol. 39 No. 3, pp. 1275-1281.

Nakamura, R. and Taniguchi, R. (1980), "Dependence of reaction times on movement patterns in patients with Parkinson's disease and those with cerebellar degeneration", *The Tohoku Journal of Experimental Medicine*, Vol. 132 No. 2, pp. 153-158.

Pandis, P., Prinold, J.A.I. and Bull, A.M.J. (2015), "Shoulder muscle forces during driving: sudden steering can load the rotator cuff beyond its repair limit", *Clinical Biomechanics*, Vol. 30 No. 8, pp. 839-846.

Pauwelussen, J.P. (2015), *Essentials of Vehicle Dynamics*, *Essentials of Vehicle Dynamics*, Elsevier, Oxford.

Pradko, F. and Lee, R.A. (1969), "Theory of human vibration response and its application to vehicle design", in Bootzin, D. and Muffley, H.C. (Eds), *Biomechanics*, Springer, New York, NY, pp. 105-118.

Rahman, H.A., Fai, Y.C. and Ming, E.S.L. (2014), "Analysis of human hand kinematics: forearm pronation and supination", *Journal of Medical Imaging and Health Informatics*, Vol. 4 No. 2, pp. 245-249.

Renfroe, D., Semones, P.T. and Roberts, A. (2007), "Quantitative measure of transient oversteer of road vehicles", *20th International Technical Conference on the Enhanced Safety of Vehicles*, *NHSTA*, *Lyon*.

Rivera, L.A. and Desouza, G.N. (2012), "A power wheelchair controlled using hand gestures, a single sEMG sensor, and guided under-determined source signal separation", *Proceedings of the IEEE RAS and EMBS International Conference on Biomedical Robotics and Biomechatronics, IEEE*, *Rome*.

Shapiro, S.S. and Wilk, M.B. (1965), "An analysis of variance test for normality (complete samples)", *Biometrika*, Vol. 52 Nos 3/4, pp. 591-611.

Sharp, R.S. and Granger, R. (2003), "On car steering torques at parking speeds", *Proceedings of the Institution of Mechanical Engineers, Part D: Journal of Automobile Engineering*, Vol. 217 No. 2, pp. 87-96.

Shimizu, Y. and Tokunaga, H. (2015), "Electric power steering system", United States Patent and Trademark Office.

Shuttleworth, M. (2009), "Counterbalanced measures design", available at: https://explorable.com/counterbalanced-measures-design (accessed 12 October 2018).

Strand, G. and Lundteigen, M.A. (2017), "On the role of HMI in human reliability analysis of offshore drilling operations", *Journal of Loss Prevention in the Process Industries*, Vol. 49, pp. 191-208.

Takada, Y., Boer, E.R. and Sawaragi, T. (2013), "Driving assist system: shared haptic human system interaction", in Narayanan, S. (Ed.), *12th IFAC Symposium on Analysis, Design, and Evaluation of Human-Machine Systems*, *International Federation of Automatic Control (IFAC)*, *Las Vegas*, pp. 203-210.

Takizawa, N., Wakita, Y., Nagata, K. and Magatani, K. (2009), "A development of the equipment control system using SEMG", in Lim, C.T. and Goh, J.C.H. (Eds), *IFMBE Proceedings*, Singapore, pp. 923-926.

Tandy, D.F., Colborn, J., Bae, J.C., Coleman, C. and Pascarella, R. (2015), "The true definition and measurement of oversteer and understeer", *SAE International Journal of Commercial Vehicles*, Vol. 8, pp. 160-181.

Tuisku, O., Surakka, V., Vanhala, T., Rantanen, V. and Lekkala, J. (2012), "Wireless face interface: using voluntary gaze direction and facial muscle activations for human-computer interaction", *Interacting with Computers*, Vol. 24 No. 1, pp. 1-9.

Upton, G. and Cook, I. (1996), *Understanding Statistics*, Oxford University Press, Oxford.

Wada, M. and Kameda, F. (2009), "A joystick car drive system with seating in a wheelchair", *2009 35th Annual Conference of IEEE Industrial Electronics, IEEE*, *Porto*, pp. 2163-2168.

Whitley, E. and Ball, J. (2002), "Statistics review 6: nonparametric methods", *Critical Care (London, England)*, Vol. 6 No. 6, pp. 509-513.

Yih, P. and Gerdes, J.C. (2005), "Modification of vehicle handling characteristics via steer-by-wire", *IEEE Transactions on Control Systems Technology*, Vol. 13 No. 6, pp. 965-976.

Corresponding author

Edric John Cruz Nacpil can be contacted at: enacpil@iis.u-tokyo.ac.jp